Solar Cells

International Edition: DOI: 10.1002/anie.201707037
German Edition: DOI: 10.1002/ange.201707037

Formation of Stable Tin Perovskites Co-crystallized with Three Halides for Carbon-Based Mesoscopic Lead-Free Perovskite Solar Cells

*Cheng-Min Tsai, Nayantara Mohanta, Chi-Yung Wang, Yu-Pei Lin, Yaw-Wen Yang, Chien-Lung Wang, Chen-Hsiung Hung, and Eric Wei-Guang Diau**

Abstract: *We synthesized and characterized methylammonium (MA) mixed tri-halide tin perovskites ($MASnIBr_{2-x}Cl_x$) for carbon-based mesoscopic solar cells free of lead and hole-transporting layers. Varied $SnCl_2/SnBr_2$ ratios yielded tin perovskites with three halides (I, Br, and Cl) co-crystallized inside the tin-perovskite. When the $SnCl_2$ proportion was $\geq 50\,\%$ ($x \geq 1$), phase separation occurred to give $MASnI_{3-y}Br_y$ and $MASnCl_{3-z}Br_z$ in the stoichiometric proportions of their precursors, confirmed by XRD. A device with $MASnIBr_{1.8}Cl_{0.2}$ ($SnCl_2 = 10\,\%$) showed the best photovoltaic performance: $J_{SC} = 14.0\ mA\,cm^{-2}$, $V_{OC} = 380\ mV$, $FF = 0.573$, and $PCE = 3.1\,\%$, and long-term stability. Electrochemical impedance spectra (EIS) show superior charge recombination and dielectric relaxation properties for the $MASnIBr_{1.8}Cl_{0.2}$ cell. Transient PL decays showed the intrinsic problem of tin-based perovskites with average lifetimes less than 100 ps.*

Organic–inorganic lead halide perovskite (e.g., $CH_3NH_3PbI_3$) solar cells (PSCs) have attracted much attention because their device performance has progressed rapidly.[1–8] Because of a concern about conventional PSCs containing toxic lead, lead-free PSCs, such as methylammonium tin tri-iodide perovskite ($MASnI_3$) solar cells have been developed.[9–16] The problem with the pure tin PSC was its unstable device performance, such that the reported efficiencies of power conversion (PCE), 5–6 %,[9,10] were difficult to reproduce.[10] We reported the use of $SnCl_2$ instead of SnI_2 to suppress the $Sn^{2+} \rightarrow Sn^{4+}$ self-doping oxidation for a tin-rich carbon-based PSC to attain PCE 5.1 %,[17] but the active perovskite layer still contained 25 % lead because PbI_2 served as a precursor. To make stable pure tin PSCs, herein we replaced PbI_2 with $SnBr_2$ as a precursor, and varied the ratios $SnCl_2/SnBr_2$ to react with CH_3NH_3I (MAI) in equimolar proportions to synthesize pure tin perovskites.

A question arises whether Cl and I can together form nano-crystalline mixed-halide perovskites.[18–25] Although there exist many reports about the unique characteristics of $MAPbI_{3-x}Cl_x$ for PV applications,[5,22–25] Cl was treated as a dopant in a small proportion inside the core structure of the perovskite crystals. $MASnI_{3-x}Cl_x$ was reported not to form a continuous solid solution because of a large difference of ionic sizes between I and Cl,[18] but we found that the mixed tri-halide tin perovskites $MASnIBr_{2-x}Cl_x$ were produced under a condition $x \leq 0.5$. When $x \geq 1$, stable tri-halide tin perovskites were not formed; phase separation produced $MASnI_{3-y}Br_y$ and $MASnBr_zCl_{3-z}$ according to the stoichiometric proportions of their precursors (Figure 1). When these

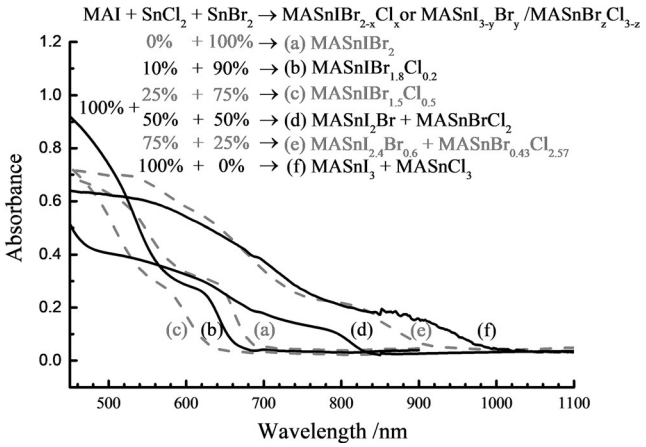

Figure 1. The synthetic approach and the absorption spectra of mixed-halide tin perovskites deposited on glass substrates with corresponding proportions of the $SnCl_2/SnBr_2$: a) 0/100; b) 10/90; c) 25/75; d) 50/50; e) 75/25; f) 100/0.

tin perovskites were fabricated into carbon-based mesoscopic solar cells, $MASnIBr_{1.8}Cl_{0.2}$ devices exhibited the best performance, PCE 3.1 %, with great reproducibility and long-term stability. Analysis of X-ray diffraction (XRD), ultraviolet photoelectron spectra (UPS), X-ray photoelectron spectra (XPS), observations with a scanning electron microscope (SEM), electrochemical impedance spectra (EIS) and transient photoluminescence (PL) decays was applied to understand the crystal structures of the unit cells and the photovoltaic performances of the devices for tin-perovskite solar cells in this series.

The mixed tri-halide tin perovskites were synthesized on mixing MAI and the $SnCl_2/SnBr_2$ precursors in equimolar proportions in DMF (Figure 1); the amount of MAI was fixed

[*] C.-M. Tsai, N. Mohanta, C.-Y. Wang, Y.-P. Lin, Dr. C.-L. Wang, Dr. E. W.-G. Diau
Department of Applied Chemistry and Institute of Molecular Science
National Chiao Tung University
Hsinchu 30010 (Taiwan)
E-mail: diau@mail.nctu.edu.tw
Dr. Y.-W. Yang
National Synchrotron Radiation Research Center
Hsinchu 30076 (Taiwan)
Dr. C.-H. Hung
Institute of Chemistry, Academia Sinica
Taipei 11529 (Taiwan)

Supporting information for this article can be found under: https://doi.org/10.1002/anie.201707037.

at 100% and the I/Br/Cl ratios were controlled on varying the $SnCl_2/SnBr_2$ concentrations with molar ratios 0/100, 10/90, 25/75, 50/50, 75/25 and 100/0. SEM/EDS analysis (Figure S1, Supporting Information) and XPS spectra (Figure S2), confirmed that the stoichiometric proportions of the $SnCl_2/SnBr_2$ mixtures gave the expected overall ratios of the mixed halides in the perovskite. Figure 1 shows absorption spectra of those mixed-halide tin perovskites deposited on glass substrates. In the case of 0% $SnCl_2$ (100% $SnBr_2$), the $MASnIBr_2$ crystal was produced with a spectral onset near 700 nm (band gap $E_g = 1.81$ eV), consistent with a report elsewhere.[9] We observed systematic blue shifts in the absorption spectra when the proportions of $SnCl_2$ was increased from 0% to 25% ($E_g = 1.97$ eV), indicating the involvement of Cl in the tin-perovskite crystal structure with an increased band gap. In contrast, when the $SnCl_2/SnBr_2$ ratio was increased to 50/50, the absorption spectrum showed a significant red shift up to about 850 nm ($E_g = 1.49$ eV); further increasing the $SnCl_2/SnBr_2$ ratios produced further red shifts of the spectra with the spectral edge approaching 1000 nm ($E_g = 1.25$ eV) at 100% $SnCl_2$. A similar spectral feature was observed for the corresponding PL spectra (Figure S3). Fine scans of the XPS plots shown in Figures S2b–e, that also display the characteristic XPS features of Sn and other halides involve a significant spectral shift toward greater binding energies upon increasing the proportions of $SnCl_2$ from 25% to 50%. The observed anomalous spectral behavior indicates that the crystal structures of the tin perovskites must be influenced significantly by the varied $SnCl_2/SnBr_2$ ratios, for which we conducted XRD analysis to solve the puzzles.

Figure 2a shows XRD patterns of mixed-halide tin perovskites prepared in varied $SnCl_2/SnBr_2$ ratios deposited on $FTO/TiO_2/Al_2O_3/C$ substrates; Figures 2b,c show the corresponding spectra expanded in two specific diffraction regions. The intense XRD features at 26.5° marked "*" are due to the carbon layer of the substrates for all devices. We observed two pronounced diffraction signals at approximately 15° and approximately 30° for the 0, 10, and 25% $SnCl_2$ samples, but these two characteristic features are split into two separate patterns; the separation of the split diffraction angles systematically increased for the 50, 75, and 100% $SnCl_2$ samples. These XRD patterns were simulated with software (TOPAS); the simulated results are shown in Figure S4, with parameters of the crystal structure summarized in Table S1.

Our XRD analysis implies three important structural features for the mixed- halide tin-perovskite crystals, summarized as follows. First, for 0% $SnCl_2$, the reaction of 100% MAI with 100% $SnBr_2$ follows a stoichiometric path to produce the $MASnIBr_2$ crystal with symmetry space group *P4mm*. Although $MASnIBr_2$ has formally a tetragonal crystal structure ($a = b \neq c$; Table S1), it is essentially pseudo-cubic with $a \approx c$. Our results are consistent with those of Yamada for a cubic crystal structure $MASnIBr_2$ with lattice parameter $a = 6.016$ Å;[18] Hao et al. reported a smaller crystal size for $MASnIBr_2$ with $a = 5.948$ Å.[9] Second, for 10 and 25% $SnCl_2$, the two characteristic diffraction features shifted slightly to larger angles, indicating that the chlorine atom is involved in the crystal structures to form contracted mixed tri-halide tin perovskites, $MASnIBr_{2-x}Cl_x$. TOPAS simulations confirmed that $MASnIBr_{1.8}Cl_{0.2}$ and $MASnIBr_{1.5}Cl_{0.5}$ were produced from 10 and 25% $SnCl_2$, respectively, with pseudo-cubic crystal structures similar to that of $MASnIBr_2$ but with smaller sizes (Table S1). The absorption spectra of the mixed-halide tin perovskites hence exhibited blue spectral shifts from 0 to 25% $SnCl_2$ (Figure 1).

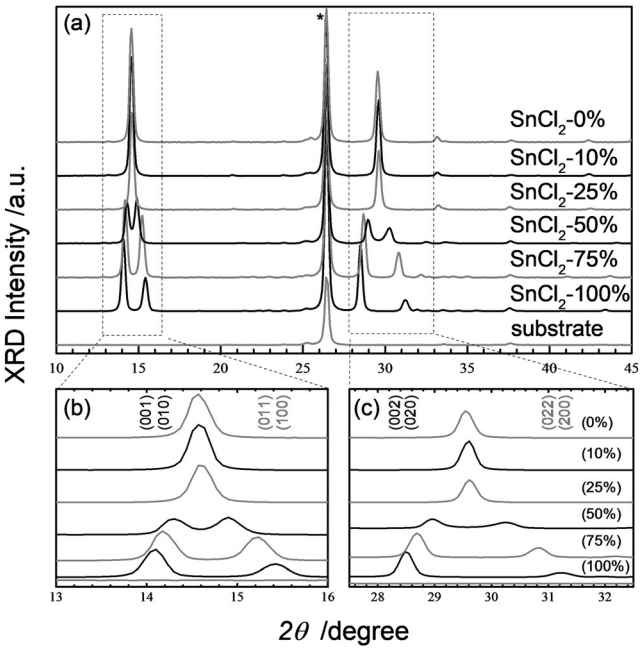

Figure 2. a) X-ray diffraction (XRD) patterns of mixed-halide tin perovskites deposited on mesoporous $FTO/TiO_2/Al_2O_3/C$ substrates with varied stoichiometric ratios of $SnCl_2/SnBr_2$ precursors. The expansions of the characteristic XRD patterns in two diffraction regions highlighted in dash-line boxes are shown in (b) and (c); Miller indices of space group *P4mm* are in black and of *P1c1* in gray. The intense XRD features marked "*" in (a) correspond to the contribution of the carbon layer of the devices.

Third, for 50–100% $SnCl_2$, the splitting of the XRD characteristic patterns shown in Figures 2b,c is due to separation of the tin perovskites into two phases; that is $MASnI_{3-y}Br_y$ (space group *P4mm*) and $MASnBr_zCl_{3-z}$ (space group *P1c1*) were produced according to the stoichiometric ratios of the precursors (Figure 1 and Table S1). Accordingly, both y and z values decreased on increasing the $SnCl_2/SnBr_2$ ratios; the lattice sizes of $MASnI_{3-y}Br_y$ (pseudo-cubic crystal structure) increased whereas the lattice sizes of $MASnBr_zCl_{3-z}$ (monoclinic) decreased upon increasing the $SnCl_2$ proportions. As shown in Figures 2b,c, upon increasing the $SnCl_2/SnBr_2$ ratios facets (001), (010), (002), and (020) of $MASnI_{3-y}Br_y$ shift systematically to smaller diffraction angles whereas facets (011), (100), (022) and (200) of $MASnBr_zCl_{3-z}$ shift systematically to larger diffraction angles. The red shifts of the absorption spectra shown in Figure 1 for the 50–100% $SnCl_2$ samples are thus explained as being due to the contributions of $MASnI_2Br$ (50% $SnCl_2$), $MASnI_{2.4}Br_{0.6}$ (75% $SnCl_2$) and $MASnI_3$ (100% $SnCl_2$) with smaller band gaps.

Yamada et al.[18] showed that tin perovskites both $MASnI_{3-y}Br_y$ ($y = 0$, 1, 2 and 3) and $MASnBr_zCl_{3-z}$ ($z = 0, 1, 2$, and 3) can form continuous solid solutions, but not $MASnI_{3-x}Cl_x$ because of the large difference of radii of I and Cl anions. Although much work is reported for their lead analogues, $MAPbI_{3-x}Cl_x$ (x representing a tiny fraction),[5,22–25] no evidence for Cl to form a solid solution together with I has been found. Lian et al.[25] used $MAPbI_3$(Cl) to form single crystal; they observed that $MAPbI_3$(Cl) exhibited greater carrier mobility and longer lifetime than those of the $MAPbI_3$ single crystal, but the amount of Cl inside the crystal was not determined. In our work, we found that Cl can co-crystallize with I in the presence of Br to form a single-phase tin-perovskite crystal such as $MASnIBr_{1.8}Cl_{0.2}$ (10% $SnCl_2$) and $MASnIBr_{1.5}Cl_{0.5}$ (25% $SnCl_2$) for which more than 50% of the halide sites in tin perovskite are occupied by Br. When the proportion of Br is less than 50%, phase separation occurs to form I/Br and Cl/Br tin perovskites according to their stoichiometric ratios. The proportion of Br hence plays a key role in the formation of stable mixed-halide tin perovskites containing three halides (I, Br, and Cl) in one crystal cell, as we observed herein.

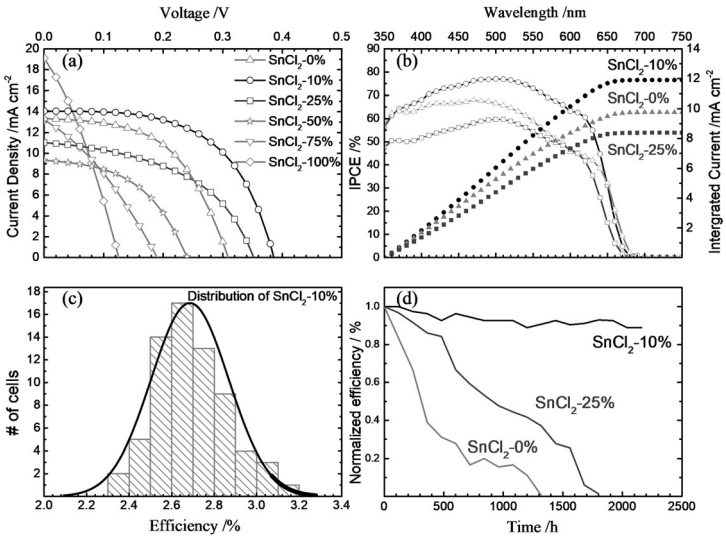

Figure 4. Photovoltaic performance of carbon-based mixed halide tin-perovskite devices showing a) current–voltage curves, b) IPCE action spectra (line + open symbols) and integrated current densities (solid symbols), c) histogram of PCE of $MASnIBr_{1.8}Cl_{0.2}$ (that is, $SnCl_2$ 10%) with 68 devices prepared under the same conditions and d) efficiency stability profiles of the encapsulated devices as a function of storage period.

Figure 3a shows the energy levels of the valence band (E_{VB}) of these mixed- halide tin perovskites deduced from the UPS (Figure S5); the energy levels of the conduction band (E_{CB}) were derived on scaling the E_{VB} levels with the corresponding E_g values evaluated from the absorption spectra (Figure 1). These tin perovskites were fabricated into carbon-based mesoscopic solar-cell devices (Figure 3b) reported elsewhere;[17] the cross-section SEM images of the corresponding tin-perovskite devices are shown in Figure S6. Figures 4a,b show J–V curves and the corresponding IPCE action spectra, respectively, for the best mixed tri-halide tin-perovskite devices; Table 1 lists the corresponding photovoltaic parameters. The photovoltaic results show the best performance for the $MASnIBr_{1.8}Cl_{0.2}$ device: $J_{SC} = 13.99\ mA\,cm^{-2}$, $V_{OC} = 380\ mV$, $FF = 0.573$, and $PCE = 3.11\%$ with a minor effect of hysteresis (Figure S7a) and stabilized output power is approximately 3.1% for a period over 100 s under one-sun irradiation (Figure S7b); this power output is significantly greater than for the $MASnIBr_2$ device ($PCE = 2.18\%$) without involving chlorine in the tin perovskite. When the proportion of Cl in perovskite was increased to form $MASnIBr_{1.5}Cl_{0.5}$, the PV performance decreased to $PCE = 1.87\%$, indicating that the proportion of Cl plays an important role to obtain the best device performance. Once phase separation occurred, the device performance became much worse than for the single-phase devices.

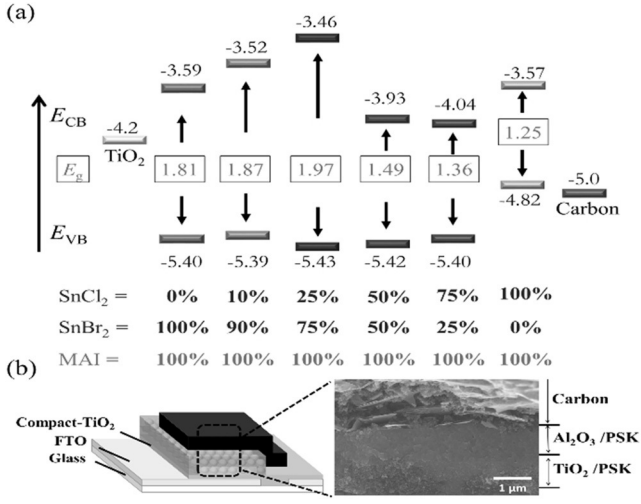

Figure 3. a) Potential-energy diagrams (energies in eV with respect to vacuum) of mixed-halide tin-perovskite films with halide ratios controlled on mixing MAI and $SnCl_2/SnBr_2$ precursors in $SnCl_2/SnBr_2$ proportions varied as indicated. b) Schematic representation of the device structure of a carbon-based perovskite solar cell with a side-view SEM image of the $MASnIBr_{1.8}Cl_{0.2}$ cell.

Sixty-eight identical $MASnIBr_{1.8}Cl_{0.2}$ devices were prepared under the same experimental conditions; the corresponding PCE histogram of these devices shown in Figure 4c indicates a narrow distribution of photovoltaic performance, spanning the range 2.3–3.2%, whereas Noel et al.[10] showed a broad distribution of PCE for the $MASnI_3$ devices. This great reproducibility implies also great stability of the devices. As shown in Figure 4d, the performance of the encapsulated $MASnIBr_{1.8}Cl_{0.2}$ device degraded only slightly and maintained 90% of the original performance after 2000 h, whereas the performance of the $MASnIBr_2$ (that is, $SnCl_2$ 0%) device degraded to zero after 1200 h.

To monitor the interfacial properties so that we can understand the trend of the device performance shown in Figure 4a, we measured EIS for these tin-perovskite devices. Nyquist plots shown in Figure S8, were fitted according to the equivalent-circuit model shown on top of the plots; the corresponding fitted parameters are listed in Table S2. For the

Table 1: Photovoltaic parameters of carbon based mixed halide perovskite devices obtained from current–voltage curves shown in Figure 4 a.

$SnCl_2$ [%]	$SnBr_2$ [%]	J_{SC} [mA cm^{-2}]	V_{OC} [mV]	FF	PCE [%]
0	100	13.37	311	0.525	2.18
10	90	13.99	380	0.573	3.11
25	75	11.06	356	0.475	1.87
50	50	9.33	241	0.474	1.07
75	25	13.34	190	0.321	0.81
100	0	19.12	125	0.309	0.74

first four devices (0–50 % $SnCl_2$), Nyquist plots feature three arcs corresponding to a charge transfer of selective contacts (high frequency), the charge recombination in the photoactive layer (intermediate frequency) and dielectric relaxation (low frequency).[26–28] First, the values of charge-transfer impedance (R_1) are similar for all devices because the n-selective contact (mesoporous TiO_2 layer) and the p-selective contact (mesoporous carbon layer) are constant for these devices. Second, the trend of charge-recombination impedance (R_2) is consistent with the trend of V_{OC} for devices in this series, which explains that the performance of the $MASnIBr_{1.8}Cl_{0.2}$ device is greater than for the other devices because of its retarded charge recombination. Third, the $MASnIBr_{1.8}Cl_{0.2}$ device has a dielectric relaxation impedance (R_3) significantly greater than that of the others, indicating that generation of photo-induced dipoles in the $MASnIBr_{1.8}Cl_{0.2}$ device was much slower than in the other devices. The retarded dielectric relaxation leads to a decreased accumulation of charge in the active perovskite layer so as to improve the effect of charge separation for the enhanced device performance.[28] The dielectric relaxation was significant for the phase-separated devices; especially for the devices made of 75 and 100 % $SnCl_2$ the dielectric relaxation might be too rapid to be observed in their Nyquist plots. As a result, small V_{OC} and FF were obtained for both two-phase devices.

We measured time-correlated single-photon counting (TCSPC) profiles for the first three mixed-halide tin perovskites with a single crystalline phase (0–25 % $SnCl_2$); the corresponding transient PL profiles appear in Figure S9. All PL transients exhibited a rapid decay feature that was fitted with three decay components, convoluted with the instrument response function (full width at half maximum (FWHM) $\approx$ 55 ps); the corresponding time coefficients (relative amplitudes in parentheses) are summarized in Table S3. The amplitudes of the first decay component dominated (A1 $\approx$ 0.98), with values of time coefficient τ_1 less than 100 ps for all three samples. The values of time coefficient τ_2 of the second decay component (A2 $\approx$ 0.02) are in the range 400–600 ps; the third decay component is negligible (A3 $\approx$ 0.003) on a ns scale. The lifetimes of tin perovskites are hence much shorter than those of the lead perovskites because of the efficient non-radiative relaxation within 100 ps. The small V_{OC} values of the devices are probably an intrinsic problem for all tin perovskites because of this rapid non-radiative carrier relaxation to lower defect states. Nevertheless, our TCSPC results indicate that the $MASnIBr_{1.8}Cl_{0.2}$ film has a lifetime greater than that of the $MASnIBr_2$ or the $MASnIBr_{1.5}Cl_{0.5}$ film, which is consistent with their corresponding device performances.

In conclusion, methylammonium mixed-halide tin perovskites were synthesized on mixing MAI and the $SnCl_2$/$SnBr_2$ precursors in equal proportions with varied $SnCl_2$/$SnBr_2$ ratios –0/100, 10/90, 25/75, 50/50, 75/25, and 100/0. The stable single-phase tin perovskites $MASnIBr_{2-x}Cl_x$ can be produced for $x \leq 0.5$; the best device performance (PCE = 3.1 %) occurred at $x = 0.2$ ($SnCl_2$/$SnBr_2$ = 10/90). When the $SnCl_2$ proportions were equal to or greater than 50 % ($x \geq 1$), both $MASnI_{3-y}Br_y$ and $MASnBr_zCl_{3-z}$ were produced according to the stoichiometric proportions of the precursors. Although continuous solid solutions $MASnI_{3-x}Cl_x$ were not formed because of the large difference of radii between I and Cl anions,[18] with more than half the halide sites being occupied by Br anions, small proportions of the halide sites can be occupied by the Cl anions to form stable tin-perovskite crystals together with three halides. The existence of Cl in a small proportion inside the tin-perovskite crystals had the effect of retarding the charge recombination, decreasing the charge accumulation, and enhancing the exciton lifetime to account for the photovoltaic performance of $MASnIBr_{1.8}Cl_{0.2}$ devices superior to that of other tin-perovskite devices.

Acknowledgements

National Synchrotron Radiation Research Center (NSRRC), Hsinchu, Taiwan, provided beam time for measurements of UPS and XPS. Ministry of Science and Technology (MOST) of Taiwan supported this work with contracts MOST105-2119-M-009-011-MY3 and MOST 105-2119-M-009-001.

Conflict of interest

The authors declare no conflict of interest.

Keywords: carbon electrodes · halides · perovskites · solar cells · tin

How to cite: *Angew. Chem. Int. Ed.* **2017**, *56*, 13819–13823
Angew. Chem. **2017**, *129*, 14007–14011

[1] A. Kojima, K. Teshima, Y. Shirai, T. Miyasaka, *J. Am. Chem. Soc.* **2009**, *131*, 6050–6051.
[2] L. Etgar, P. Gao, Z. Xue, Q. Peng, A. K. Chandiran, B. Liu, M. K. Nazeeruddin, M. Grätzel, *J. Am. Chem. Soc.* **2012**, *134*, 17396–17399.
[3] H. S. Kim, C. R. Lee, J. H. Im, K. B. Lee, T. Moehl, A. Marchioro, S. J. Moon, R. Humphry-Baker, J. H. Yum, J. E. Moser, M. Grätzel, N. G. Park, *Sci. Rep.* **2012**, *2*, 591.
[4] M. M. Lee, J. Teuscher, T. Miyasaka, T. N. Murakami, H. J. Snaith, *Science* **2012**, *338*, 643–647.

[5] C. Wehrenfennig, G. E. Eperon, M. B. Johnston, H. J. Snaith, L. M. Herz, *Adv. Mater.* **2014**, *26*, 1584 – 1589.
[6] N. Ahn, D. Y. Son, I. H. Jang, S. M. Kang, M. Choi, N. G. Park, *J. Am. Chem. Soc.* **2015**, *137*, 8696 – 8699.
[7] *Organic-Inorganic Halide Perovskite Photovoltaics: From Fundamentals to Device Architectures*, (Eds.: N. G. Park, M. Grätzel, T. Miyasaka), Springer International Publishing, Amsterdam, **2016**.
[8] J.-P. Correa-Baena, A. Abate, M. Saliba, W. Tress, T. Jesper Jacobsson, M. Grätzel, A. Hagfeldt, *Energy Environ. Sci.* **2017**, *10*, 710 – 727.
[9] F. Hao, C. C. Stoumpos, D. H. Cao, R. P. H. Chang, M. G. Kanatzidis, *Nat. Photonics* **2014**, *8*, 489 – 494.
[10] N. K. Noel, S. D. Stranks, A. Abate, C. Wehrenfennig, S. Guarnera, A.-A. Haghighirad, A. Sadhanala, G. E. Eperon, S. K. Pathak, M. B. Johnston, A. Petrozza, L. M. Herz, H. J. Snaith, *Energy Environ. Sci.* **2014**, *7*, 3061 – 3068.
[11] F. Hao, C. C. Stoumpos, P. Guo, N. Zhou, T. J. Marks, R. P. H. Chang, M. G. Kanatzidis, *J. Am. Chem. Soc.* **2015**, *137*, 11445 – 11452.
[12] T. Yokoyama, D. H. Cao, C. C. Stoumpos, T. B. Song, Y. Sato, S. Aramaki, M. G. Kanatzidis, *J. Phys. Chem. Lett.* **2016**, *7*, 776 – 782.
[13] H. Do Kim, Y. Miyamoto, H. Kubota, T. Yamanari, H. Ohkita, *Chem. Lett.* **2017**, *46*, 253 – 256.
[14] T. Fujihara, S. Terakawa, T. Matsushima, C. Qin, M. Yahiro, C. Adachi, *J. Mater. Chem. C* **2017**, *5*, 1121 – 1127.
[15] T. B. Song, T. Yokoyama, C. C. Stoumpos, J. Logsdon, D. H. Cao, M. R. Wasielewski, S. Aramaki, M. G. Kanatzidis, *J. Am. Chem. Soc.* **2017**, *139*, 836 – 842.
[16] T. Yokoyama, T.-B. Song, D. H. Cao, C. C. Stoumpos, S. Aramaki, M. G. Kanatzidis, *ACS Energy Lett.* **2017**, *2*, 22 – 28.
[17] C.-M. Tsai, H.-P. Wu, S.-T. Chang, C.-F. Huang, C.-H. Wang, S. Narra, Y.-W. Yang, C.-L. Wang, C.-H. Hung, E. W.-G. Diau, *ACS Energy Lett.* **2016**, *1*, 1086 – 1093.
[18] K. Yamada, K. Nakada, Y. Takeuchi, K. Nawa, Y. Yamane, *Bull. Chem. Soc. Jpn.* **2011**, *84*, 926 – 932.
[19] S. Colella, E. Mosconi, P. Fedeli, A. Listorti, F. Gazza, F. Orlandi, P. Ferro, T. Besagni, A. Rizzo, G. Calestani, G. Gigli, F. De Angelis, R. Mosca, *Chem. Mater.* **2013**, *25*, 4613 – 4618.
[20] H. Yu, F. Wang, F. Xie, W. Li, J. Chen, N. Zhao, *Adv. Funct. Mater.* **2014**, *24*, 7102 – 7108.
[21] M. I. Dar, N. Arora, P. Gao, S. Ahmad, M. Grätzel, M. K. Nazeeruddin, *Nano Lett.* **2014**, *14*, 6991 – 6996.
[22] J. Chae, Q. Dong, J. Huang, A. Centrone, *Nano Lett.* **2015**, *15*, 8114 – 8121.
[23] Q. Chen, H. Zhou, Y. Fang, A. Z. Stieg, T. B. Song, H. H. Wang, X. Xu, Y. Liu, S. Lu, J. You, P. Sun, J. McKay, M. S. Goorsky, Y. Yang, *Nat. Commun.* **2015**, *6*, 7269.
[24] Y. Chen, T. Chen, L. Dai, *Adv. Mater.* **2015**, *27*, 1053 – 1059.
[25] Z. Lian, Q. Yan, T. Gao, J. Ding, Q. Lv, C. Ning, Q. Li, J. L. Sun, *J. Am. Chem. Soc.* **2016**, *138*, 9409 – 9412.
[26] J. Bisquert, L. Bertoluzzi, I. Mora-Sero, G. Garcia-Belmonte, *J. Phys. Chem. C* **2014**, *118*, 18983 – 18991.
[27] R. S. Sanchez, V. Gonzalez-Pedro, J. W. Lee, N. G. Park, Y. S. Kang, I. Mora-Sero, J. Bisquert, *J. Phys. Chem. Lett.* **2014**, *5*, 2357 – 2363.
[28] C.-C. Chung, S. Narra, E. Jokar, H.-P. Wu, E. W.-G. Diau, *J. Mater. Chem. A* **2017**, *5*, 13957 – 13965.

Manuscript received: July 11, 2017
Accepted manuscript online: September 5, 2017
Version of record online: September 22, 2017

